EarthArXiv preprint cover sheet

This is a non-peer-reviewed preprint submitted to EarthArXiv. It has been submitted for publication in *Communications Earth & Environment* (Nature Portfolio). Subsequent peer-reviewed versions may differ from this manuscript; if accepted, the final version-of-record will be available via a DOI link on this preprint page. Feedback is welcome and may be sent to the corresponding author.

Per-tree leaf area index mapping of Amsterdam's unrecorded shade canopy

Théo Alessandro Hermann[1,2], Michiel van Selm[1,2], Titus Venverloo[1,2], Fabio Duarte[1], Carlo Ratti[1,3]

[1] MIT Senseable City Lab, Massachusetts Institute of Technology, Cambridge, MA, USA
[2] Amsterdam Institute for Advanced Metropolitan Solutions (AMS Institute), Amsterdam, The Netherlands
[3] Politecnico di Milano, Milan, Italy

Corresponding author: Théo Alessandro Hermann (thermann@mit.edu)

Code and data. Code and the per-tree dataset are released upon publication at:

- Code: `https://github.com/thrmnn/invisible-forest`
- Data: `https://huggingface.co/datasets/thrmnn/invisible-forest-amsterdam`

Contents. This combined PDF contains the main manuscript followed by the Supplementary Information. EarthArXiv does not host separate supplementary files; the code repository and dataset above hold the reproducible materials.

Per-tree leaf area index mapping of Amsterdam's unrecorded shade canopy

Théo Alessandro Hermann[1,2*], Michiel van Selm[1,2], Titus Venverloo[1,2], Fabio Duarte[1], Carlo Ratti[1,3]

[1]Senseable City Lab, Massachusetts Institute of Technology, 77 Massachusetts Avenue, Cambridge, USA.
[2]Amsterdam Institute for Advanced Metropolitan Solutions, Kattenburgerstraat 5, Amsterdam, Netherlands.
[3]ABC Department, Politecnico di Milano, Milan, Italy.

*Corresponding author(s). E-mail(s): thermann@mit.edu;
Contributing authors: mvanselm@mit.edu; tvenver@mit.edu; fduarte@mit.edu; ratti@mit.edu;

Abstract

Most of the trees shading Amsterdam are absent from any municipal record. Using the Dutch national LiDAR survey (AHN5), we derive per-tree Leaf Area Index for nearly 850,000 trees across 243 $\mathbf{km^2}$. Roughly 62% of the canopy is unrecorded, and these unregistered trees carry a disproportionate share (about two-thirds) of the city's gross shade, so most of this shade-providing canopy lies outside the systems meant to manage it. Uniform-transmissivity models correctly diagnose *where* shade is scarce ($\boldsymbol{\rho = 0.997}$) but not *what* produces it: measured per-tree canopy transmission averages several times the single value they assume (bounded $\approx$2–4$\times$), and the densest genus casts 11% more shade per crown than the sparsest. Within-neighbourhood density variation adds up to 5.7 percentage points of shade (2.8 on average) that averaged models erase. Ninety-five percent of neighbourhoods fall below the 30% canopy-cover target. Comparable national LiDAR across Europe and the US suggests the method is transferable, pending validation at other point densities and canopy types.

Keywords: Urban Trees, Leaf Area Index, Urban Heat Island, Shade Equity, LiDAR, Urban Forest Inventory

Shade is the most effective passive cooling strategy available to cities confronting escalating urban heat [1]. Tree canopies reduce mean radiant temperature by up to 20°C [2] and ambient air temperature by 0.5–2.0°C [3], with the magnitude of cooling depending strongly on species-specific canopy traits including leaf area density, crown architecture, and transpiration rate [4–6]. With urban heat driving thousands of excess deaths annually in Europe [7], the World Health Organization links urban green space to health [8], the widely adopted 3-30-300 rule sets a minimum 30% neighbourhood canopy cover [9], and the EU Nature Restoration Regulation now requires Member States to prevent net loss of urban tree canopy by 2030 [10]: a mandate demanding monitoring infrastructure most cities do not yet possess.

The spatial diagnosis of shade inequality is now well established. Environmental justice research has documented unequal distribution of urban tree cover along income lines [11–13], and Gu et al. recently quantified this pattern across nine global cities (including Amsterdam), demonstrating that shade on pedestrian surfaces is persistently and unequally distributed [14]. Yet knowing *where* shade is unequal tells cities nothing about *what* produces the inequality, whether they *know* the trees responsible, or how to design species-specific interventions that close the gap: the transition from diagnosis to prescription demands canopy resolved tree by tree. Two structural limitations, shared by all city-scale shade assessments to date, prevent that transition. First, every such assessment treats canopy as uniformly opaque: Gu et al. applied a uniform transmissivity of $\tau = 0.10$ [14]; similar assumptions appear in shade decompositions [15] and radiation models [16]. Second, these assessments rely on municipal tree registers, asset-management tools that record what the city planted on public land [17, 18], and therefore systematically exclude private gardens and self-seeded growth [19, 20].

Both limitations have mechanistic consequences. The density of a canopy (its Leaf Area Index, LAI, defined as one-sided leaf area per unit ground area [21]) governs radiation interception through the Beer–Lambert law, and crown transmissivity varies across genera: published measurements span a 7-fold range [22]. Whether this variation persists under real urban growing conditions has not been tested at city scale. A neighbourhood at 25% canopy cover with dense canopies receives different shade than one at 25% cover with open canopies, yet current metrics treat them identically. The register-incompleteness limit has a parallel character: comparative studies across Nordic cities demonstrate that register completeness varies widely even among data-rich municipalities [23, 24], suggesting the visibility gap is structural rather than city-specific, a pattern recognised globally by the FAO's Trees Outside Forests framework [25].

Here we address both limitations, exploiting the Netherlands' AHN5 national airborne LiDAR campaign to derive per-tree canopy density (LAI) for 846,985 trees across the entire 243 km^2 Amsterdam municipality [26, 27]. The AHN programme has been processed into national-scale ecosystem products at 10 m resolution [28], and prior work mapped grid-level LAI across Gothenburg at comparable resolution [29]; our approach resolves LAI to individual crowns, enabling species-resolved transmissivity and per-tree shade attribution. Three contributions follow. First, 62% of the

urban canopy ($n = 526{,}499$) is absent from any municipal record, yet these unregistered trees deliver a disproportionate share of the city's shade (about two-thirds of citywide shade), revealing that the majority of Amsterdam's shade-providing canopy is invisible to the governance systems designed to maintain it. Second, measured per-tree transmissivity averages about threefold the uniform value $\tau = 0.10$ used in global models, and within-neighbourhood LAI variance produces an additional shade contribution (a Jensen gap averaging $+2.8$ pp across 484 neighbourhoods, $R^2 = 0.987$ against second-order theory) that any uniform-density model is mathematically blind to regardless of its calibration. Third, the per-tree database enables species-specific planting prescription and tree-level protection: in many neighbourhoods the top-decile shade trees are disproportionately unregistered, identifying which existing trees merit legal protection before development and which species to plant where: prescriptive questions aggregate metrics cannot answer.

1 Results

1.1 A complete urban tree database

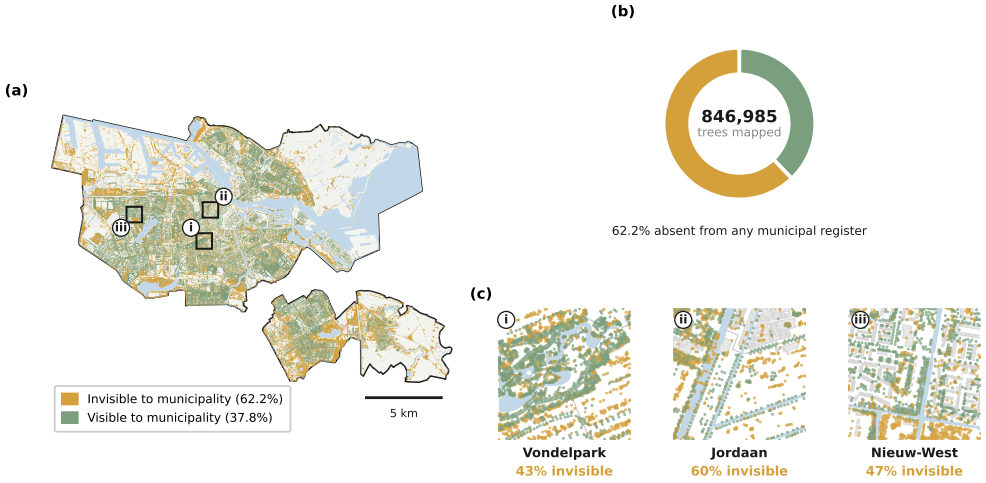

Fig. 1: **Amsterdam's urban forest is largely invisible to municipal monitoring. a,** Spatial distribution of 846,985 trees detected from AHN5 LiDAR across the 243 km^2 Amsterdam municipality, coloured by registration status: visible to the municipality (green, 37.8%) and absent from any municipal register (amber, 62.2%); surface water is shown in pale blue. **b,** Database composition showing that the majority of the urban canopy exists outside any municipal management system. **c,** Neighbourhood insets illustrating three contrasting spatial patterns: Vondelpark (43% invisible), Jordaan (historic centre, 60% invisible, predominantly private garden trees), and Nieuw-West (suburban mix, 47% invisible).

The merged database contains 846,985 trees, more than 2.6× the 320,486 trees in the BOMEN 2026 municipal register (Fig. 1). This count and the invisibility fraction depend on detection-pipeline parameters (5 m matching radius, 8 m^2 minimum crown, 2 m height threshold; see Methods); a wider or tighter radius shifts both by several percentage points (detection-pipeline yield in Extended Data Fig. 1). Sixty-two percent of the canopy (62.2%, $n = 526{,}499$) is absent from any municipal inventory: trees in private gardens and self-seeded growth. A further 25.2% ($n = 213{,}438$) are confirmed by both LiDAR detection and register records, and 12.6% ($n = 107{,}048$) appear only in the register, predominantly recent plantings below the 2 m height detection threshold or entries with positional errors exceeding the 5 m matching radius. Three neighbourhood insets (Fig. 1c) illustrate how the invisible fraction stays high across contrasting urban fabrics: 43% around the Vondelpark, 47% in suburban Nieuw-West, and 60% in the historic Jordaan, where private gardens behind canal houses harbour canopy that no municipal database documents. The majority of Amsterdam's shade-providing canopy is absent from the municipal monitoring systems designed to track it.

1.2 City-scale Leaf Area Index

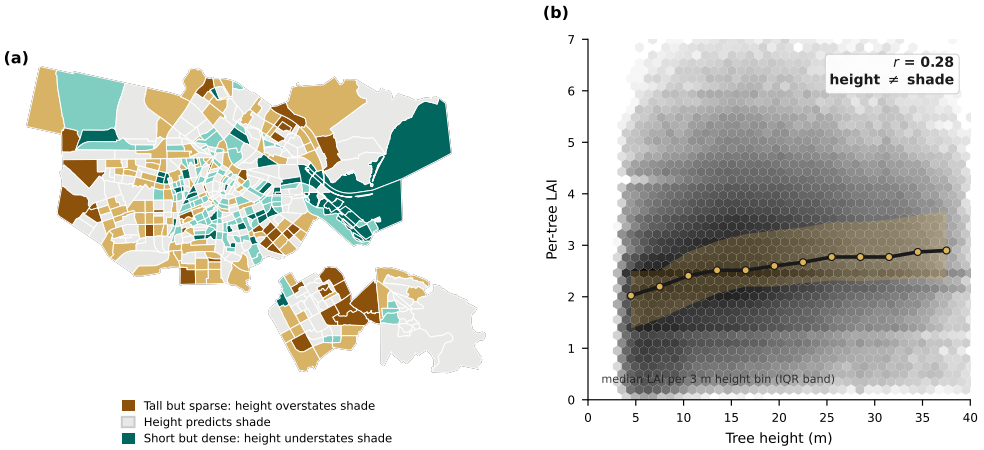

Fig. 2: **Per-tree LAI reveals what height cannot. a,** Height–LAI mismatch by neighbourhood (mean tree-height tercile minus mean-LAI tercile). Brown: taller than its density implies, so height overstates shade; green: denser than its height implies, so height understates shade; grey: height tracks shade. The two diverge in 58% of neighbourhoods. **b,** Per-tree LAI against tree height (grey density); the median LAI per 3 m height bin (line, with inter-quartile band) stays nearly flat ($r \approx 0.3$), confirming height is a poor proxy for canopy density.

Citywide mean LAI is 2.54 (median 2.51, s.d. 0.92), with mean crown transmissivity (the fraction of incoming sunlight that passes through the canopy) of $\tau = 0.311$

under the central extinction coefficient ($k_{\text{solar}} = 0.5$), indicating that roughly 69% of incoming solar radiation is intercepted by tree canopies. These values represent effective plant area index (PAI_e); relative rankings across trees and neighbourhoods are stable under parameter perturbations (Extended Data Figs. 2b, 5), but absolute LAI and τ magnitudes are model-dependent and should be interpreted as bounded estimates (see Methods). LAI is derived directly from the AHN5 LiDAR rasters for every detected tree (Methods). The correlation between LAI and tree height is weak (Fig. 2b), confirming that height alone is a poor proxy for shade capacity. Mapping this mismatch by neighbourhood (Fig. 2a) shows height overstating shade in tall-but-sparse areas and understating it in short-but-dense ones, so height- and area-based metrics misrank shade provision. Woody elements contribute 10–15% of total PAI_e in broadleaf leaf-on canopies [30], and genus rank order is invariant to the leaf-fraction assumption (Extended Data Fig. 5).

1.3 The Jensen gap: within-neighbourhood variance that uniform models cannot see

Uniform-transmissivity models face a more fundamental limitation than magnitude miscalibration: they cannot see within-neighbourhood LAI variance at all. Because the shade function is concave (each additional unit of LAI adds less shade than the last), a neighbourhood where some trees are very dense and others are sparse produces more total shade than one where every tree has the average density. This mathematical property (Jensen's inequality, applied to the Beer–Lambert function $1 - e^{-k \cdot \text{LAI}}$) means that LAI variance itself is a shade resource that uniform models erase. We quantify this effect across 484 neighbourhoods containing $\geq$50 trees each. The empirical Jensen gap (actual shade minus shade predicted from mean LAI alone) averages +2.8 percentage points across these 484 neighbourhoods, reaching nearly 6 pp in the highest-variance cases, and tracks within-neighbourhood LAI variance with a Pearson correlation of 0.88. The second-order Taylor expansion $\frac{1}{2}k^2 e^{-k\mu}\text{Var}(\text{LAI})$ matches the empirical gap with $R^2 = 0.987$ (Fig. 3b), confirming the mechanism is purely a consequence of functional concavity.

A matched-mean example makes the effect concrete. Three neighbourhoods at the same mean LAI ($\approx$2.28) but rising variance, Reigersbos 1 (CV = 0.09), Sportpark Middenmeer-Zuid (CV = 0.36), and Reigersbos 3 (CV = 0.48), deliver Jensen gaps that climb from +0.16 to +2.80 to +4.90 pp (Fig. 3a). Uniform-τ models return the same answer for all three; the per-tree measurement reveals materially different shade. The effect is invisible to any model that aggregates LAI to a neighbourhood mean before computing transmissivity, regardless of how well-calibrated the uniform τ value is. For planners, a mix of densities yields more shade than uniform planting at equal cover: density diversity, not amount alone, is a shade lever.

1.4 Species-resolved shade supply

Per-tree LAI reveals crown transmissivity ranging from $\tau = 0.26$ (Populus) to $\tau = 0.33$ (Prunus) across genus means: about a 30% range. The citywide per-tree mean transmissivity is about three times the uniform $\tau = 0.10$, bounded $\approx$2.2–4.3$\times$ under joint

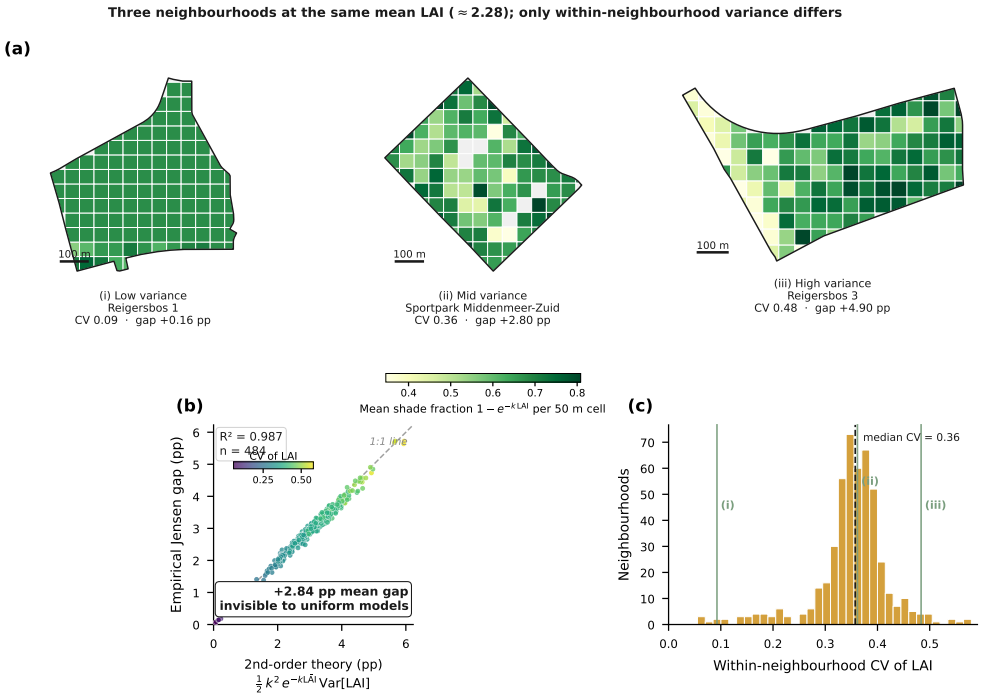

Fig. 3: **Within-neighbourhood LAI variance is a shade resource that uniform-transmissivity models are mathematically blind to.** The shade fraction $1 - e^{-k \cdot \mathrm{LAI}}$ is a concave function of canopy density: each additional unit of LAI adds less shade than the last. By Jensen's inequality, a neighbourhood that mixes dense and sparse trees therefore produces *more* total shade than one where every tree carries the neighbourhood-mean density: the variance itself contributes shade. The empirical Jensen gap quantifies this contribution: it is the difference between actual shade (averaged over the per-tree LAI distribution) and the shade a uniform model returns when applied to the neighbourhood mean. **a,** Three neighbourhoods matched on mean LAI (≈2.28) but spanning a range of within-neighbourhood variance: Reigersbos 1 (CV = 0.09), Sportpark Middenmeer-Zuid (CV = 0.36), and Reigersbos 3 (CV = 0.48). Holding the mean fixed isolates variance as the only difference, yet the empirical Jensen gap climbs from +0.16 to +2.80 to +4.90 pp. Tile maps show per-cell shade fraction; the relationship also holds at the 50 m cell scale (Spearman $\rho = 0.96$). **b,** The mechanism is purely a consequence of concavity. Across 484 neighbourhoods (≥50 trees each), the empirical Jensen gap matches the second-order Taylor expansion $\frac{1}{2}k^2 e^{-k\mu}\mathrm{Var}(\mathrm{LAI})$ at $R^2 = 0.987$, i.e. the variance term alone explains nearly all of the gap. **c,** Within-neighbourhood CV of LAI across the 484 qualifying neighbourhoods (median CV = 0.36); the three exemplars span the distribution's low (0.09), middle (0.36), and high (0.48) range.

parameter uncertainty (absolute values model-dependent; see Methods). Applying

uniform $\tau = 0.10$ to our database preserves neighbourhood shade rankings almost perfectly (Spearman $\rho = 0.997$) but overestimates absolute shade by 17–45% depending on the assumed extinction coefficient (Extended Data Fig. 4). Identical rankings need not imply identical prescriptions: uniform models *diagnose* which neighbourhoods are shade-deprived, but per-tree LAI is required to calibrate intervention magnitude and to reveal the within-neighbourhood variance of Fig. 3. At equal crown area, choosing the densest available genus over the sparsest delivers 11% more shade per crown, a species-selection lever uniform models erase. Headline ESA quantities below are reported as gross shadow footprints (per-tree shadow areas summed without subtracting overlap with building shadows or among trees); net tree shade (the building-overlap-subtracted quantity) is reported separately below. Gross Effective Shade Area (ESA; time-integrated, irradiance-weighted shadow footprints on 3 August 2024, Amsterdam's peak urban heat-island day; see Methods) is dominated by the unregistered canopy: unregistered trees contribute about two-thirds of gross citywide ESA (Fig. 1), broadly in line with their share of the tree count. Net tree shade totals 7,281 ha (54.3% of gross tree shadow; 48.3% marginal contribution beyond buildings). Shadow geometry is resolved for the LiDAR-detected canopy that casts the shade; because the unregistered fraction is itself detected canopy and we report registration *shares* rather than absolute totals, ESA-based shares are comparative across categories (see Methods).

1.5 Canopy deficit, protection gaps, and heat vulnerability

Across 516 neighbourhoods containing trees, 491 (95.2%) fall below the 30% canopy-cover target of the 3-30-300 rule [9] and 423 (82%) fall below 20%; mean canopy cover is 13.6% (crown-polygon area over land, excluding water; not pixel-identical with satellite products). This places Amsterdam among the many dense cities that fall short of the 30% threshold [31], reflecting historic urban form as much as planting policy. The Shade Gap Index quantifies the resulting shortwave-radiation deficit relative to an unshaded baseline (see Methods). The worst-served neighbourhoods are in the historic city centre and postwar housing estates, where dense built form and limited planting space combine to create acute shade deficits.

Protection gap.

Per-tree LAI enables a prescriptive policy question that uniform or aggregate metrics cannot answer: which *individual* trees carry the most shade, and does the municipality formally protect them? Ranking trees by shade contribution and cross-referencing registration status shows that in many neighbourhoods the highest-shade trees are disproportionately unregistered: the best shade comes from the least protected canopy (Fig. 4b). The IJ waterfront development zones in northern Amsterdam show the clearest inversion: newly built areas where registered street trees are still young, while the best shade comes from mature canopy on adjacent land the municipality has no mandate to replace if lost. This kind of analysis requires knowing both the location and the canopy density of every tree, information that no register or lookup table contains.

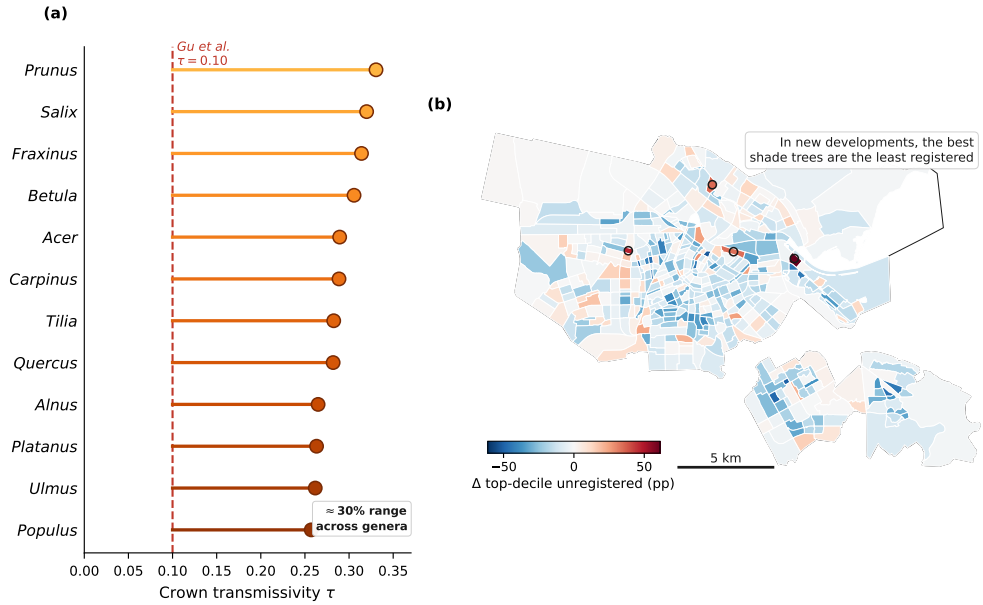

Fig. 4: **Per-tree resolution enables policy levers that uniform models cannot support. a,** Genus-mean crown transmissivity for the twelve most common genera, from Populus ($\tau = 0.26$) to Prunus ($\tau = 0.33$): about a 30% range that the uniform model ($\tau = 0.10$; dashed line) erases. Absolute τ is model-dependent (see Methods). **b,** Protection-gap map: per-neighbourhood deviation of the top-decile shade trees' unregistered fraction (trees ranked by gross ESA) from the citywide baseline. Red marks neighbourhoods where the top-decile trees are disproportionately *more* unregistered than the baseline; blue marks the opposite. The annotated IJ-waterfront clusters are the clearest case: in new development zones the best shade trees are the ones the city has no formal mandate to protect.

Heat vulnerability and income.

A three-component Heat Vulnerability Index (UHI exposure, canopy deficit, elderly population share [32]) identifies Nieuwmarkt (HVI = 1.40), Anjeliersbuurt-Zuid (1.34), and Harmoniehofbuurt (1.20) as the most vulnerable neighbourhoods (Extended Data Fig. 6). These top-3 rankings are stable across alternative weighting schemes (Spearman $\rho = 0.74$); the full Q5 list (73 neighbourhoods) serves as indicative screening rather than definitive ranking.

Canopy cover correlates weakly with socioeconomic status (bijstand rate $r = +0.17$, Spearman $\rho = +0.22$; housing value $r = -0.16$, $\rho = -0.31$; CBS income is suppressed, so bijstand rate proxies poverty), in contrast to the positive income–canopy relationship documented across US cities [11]. These proxies are censored and the associations are weak, so we read them as a near-null income gradient rather than positive evidence of equity. Amsterdam's shade deficit reflects built-form constraints

(historic-centre density, postwar housing typology) that cut across income strata (see Discussion).

2 Discussion

2.1 The invisible forest as a governance visibility gap

That 62% of a European capital's shade-producing canopy is unmonitored exposes a structural governance gap, sharpened by the finding that these invisible trees deliver about two-thirds of the city's shade. Municipal registers are asset-management tools for publicly maintained trees [18, 33], not ecological inventories of the functional canopy. The distinction between trees cities *own* and trees cities *depend on* has been noted conceptually [17] but never quantified at city scale. Unregistered trees receive no maintenance budget, no management plan, and no replacement obligation; visibility is the prerequisite for protection.

Amsterdam's Bomenverordening requires a felling permit for any tree with trunk circumference $\geq$31 cm regardless of land ownership [34], yet over 5,000 private trees are felled annually with 92–96% of permits approved and replanting obligations weakly enforced [35]. The gap is monitoring, not regulation: the city cannot enforce what it cannot see [36].

Register incompleteness is structural, not city-specific: US urban forests are 15–35% larger than inventory-based estimates [19], and trees outside forests are systematically excluded from national accounting [20]. Our 62% figure quantifies at city scale what these studies inferred. The regulatory urgency is continental: the EU Nature Restoration Regulation mandates no net loss of urban canopy by 2030 [10] at a monitoring resolution most municipalities cannot provide, and register data alone will systematically misrepresent actual coverage [37]. National LiDAR programmes (AHN, UK Environment Agency, USGS 3DEP) make replication feasible where comparable data exist, pending validation at their point densities.

2.2 What per-tree data change: from diagnosis to prescription

The near-perfect rank preservation ($\rho = 0.997$) between uniform and per-tree models raises a legitimate question: if both identify the same shade-deprived neighbourhoods, what does per-tree LAI change? The answer turns on two stages of shade policy. *Diagnosis*, which neighbourhoods need more shade, is tractable with uniform models, satellite canopy cover, or visual inspection. *Prescription*, how many trees of which species to plant and which to protect, is what uniform models cannot answer regardless of calibration.

A worked example makes this concrete (central-k estimates; see Limitations). Nieuwmarkt, the most heat-vulnerable neighbourhood (HVI = 1.40, ~8% canopy), needs ~4,300 m^2 of new crown to halve its deficit to the 20% target. Under uniform $\tau = 0.10$ this canopy would block 90% of incoming radiation, but per-tree yield depends on species: Populus ($\tau = 0.26$) delivers ~18% less shade than predicted and Prunus ($\tau = 0.33$) ~26% less, so planners must plant 21–35% more trees than

the area-based prescription suggests, a species-selection lever uniform models erase entirely.

Per-tree data expose a second dimension uniform models cannot see: the shade contribution of within-neighbourhood density variation. Because shade is a concave function of canopy density, mixing dense and sparse trees produces more total shade than uniform-density planting: Jensen's inequality applied to the Beer–Lambert function (Fig. 3). The gap averages +2.8 pp across 484 neighbourhoods, reaching nearly 6 pp in the highest-variance cases. Uniform models therefore underestimate shade in high-variance neighbourhoods, potentially misdirecting resources toward areas that already self-mitigate. Maintaining diversity of canopy density, not just canopy cover, is itself a shade resource only per-tree measurement can see.

A third capacity is protection: in many neighbourhoods the top-decile shade trees are disproportionately unregistered, so the most important trees for shade are those the municipality has least authority to preserve (Fig. 4b). The IJ waterfront shows the inversion (young registered street trees beside mature, unprotected canopy), and identifying it requires per-tree location and density that no register contains.

For cities without LiDAR, satellite-derived canopy cover supports the diagnostic layer; per-tree resolution becomes valuable precisely when a city moves from knowing where shade is lacking to deciding what to do about it.

2.3 Amsterdam's shade deficit tracks built form more than income

Prescription capacity does not guarantee equitable outcomes; Amsterdam's shade deficit appears shaped more by built form than by planting resources or income. Canopy cover correlates only weakly with socioeconomic status (bijstand rate $r = +0.17$, $\rho = +0.22$; housing value $r = -0.16$, $\rho = -0.31$), in contrast to the positive income–canopy relationship documented across US cities [11, 12]: the historic centre combines the highest property values with the deepest shade deficits. On these censored proxies we cannot detect a strong income gradient; the deficit instead concentrates in dense built forms, suggesting intervention should prioritise those neighbourhoods irrespective of their income profile. Greening high-value, high-deficit neighbourhoods nonetheless risks "green gentrification" [38, 39], documented for Amsterdam [40], so planting in priority neighbourhoods should be paired with affordability safeguards.

2.4 Limitations

Relative accuracy (well supported).

The paper's policy conclusions depend on relative rankings, stable across all perturbations examined: which neighbourhoods are shade-deprived, which genera are denser, where variance-driven gaps occur, and which trees to protect. Monte Carlo sensitivity ($n = 1{,}000$ simultaneous draws of LAI, k, solar elevation, and default τ, each $\pm 20\%$) yields neighbourhood rank $\rho = 0.93$; the k-sweep preserves genus-level rank at $\rho = 0.976$ with no line crossings; woody-fraction correction leaves genus rank invariant ($\rho = 1.000$ across all α, Extended Data Fig. 5).

Absolute accuracy (bounded but uncertain).

Absolute LAI and τ magnitudes carry systematic uncertainty that constrains absolute shade estimates without affecting comparative conclusions. The LiDAR-derived metric is effective plant area index (PAI_e), in which woody elements contribute 10–15% in broadleaf leaf-on canopies [30]; raster-derived PAI_e sits $\sim$2.4 units below published species references (Extended Data Fig. 2a), an approximately additive offset that preserves genus rank. Hemispherical photography on five Ulmus trees (RMSE = 0.86) confirms physical plausibility but is limited to a single genus and season, within the inter-method variability (CV $>$ 30%) documented for isolated urban trees [41]. Field campaigns across genera and seasons, and empirical k from multi-angular LiDAR [42], would bracket absolute values more tightly.

Gross vs net shade attribution.

The headline ESA share, the 67% from unregistered trees, is a *gross* per-tree shadow footprint, not subtracting overlap with building shadows; net tree shade, which does, totals 7,281 ha. On a net basis the unregistered share would fall below 67%, because unregistered trees concentrate in the dense-shadowed historic centre and inner districts, so more of their gross shadow falls on already-shaded ground. We report gross ESA because it compares cleanly across registration categories; the comparative claim, that unregistered trees deliver a disproportionate share of canopy shade, holds either way, and only absolute magnitudes shift.

Other caveats.

The Beer–Lambert framework omits transpirational cooling (10–30% of total tree cooling) [43]; our shade results address radiation interception only. The ESA model sums per-tree shadows independently, so inter-tree mutual shading is not subtracted, modestly overestimating shade in dense stands. AHN5 captures a single leaf-on state, so we restrict ESA reporting to one peak-summer date (3 August 2024) and leave deciduous dynamics uncharacterised. Amsterdam's flat terrain, temperate broadleaf canopy, and high-density LiDAR (25 pts/m^2) are favourable conditions; absolute-accuracy bounds require local validation elsewhere.

3 Methods

3.1 Study area and data

The study covers the entire Amsterdam municipality (52.37°N, 4.90°E) using fourteen Kadaster tiles (each 5 × 6.25 km), together spanning the full 243 km^2 municipal area.

Airborne LiDAR data were obtained from the AHN5 national campaign (Actueel Hoogtebestand Nederland, acquired 2020–2022) at a mean density of 25 pts/m^2. The AHN programme has previously been processed into national-scale ecosystem structure products at 10 m resolution [28]; our pipeline extends this to individual-tree resolution. Canopy height models (CHM) at 0.5 m resolution were derived by subtracting the digital terrain model from the digital surface model, both distributed by PDOK. LAI rasters at matching 0.5 m resolution were computed via Beer–Lambert

inversion of LiDAR penetration ratios (see Leaf Area Index Extraction). Aerial imagery from the Kadaster (0.25 m, four-band RGB and colour-infrared) was used to compute NDVI for vegetative filtering.

The municipal BOMEN register (2026 release) provides 320,486 public trees with species identification, height class, crown diameter, and planting year. CBS neighbourhood boundaries define 519 statistical areas, of which 516 contain at least one detected tree. UHI data were obtained from RIVM at 10 m resolution. 3D building models from the 3D BAG (3D register of all buildings in the Netherlands, LOD2 detail) provide roof heights for shadow computation. All data were projected to EPSG:28992 and clipped to the Amsterdam municipality boundary.

Temporal alignment spans approximately two to three years (LiDAR 2020–2022, aerial imagery July 2023, BOMEN register cumulative). For mature urban trees, annual crown growth of 0.1–0.3 m represents less than 2% of mean crown diameter, and the large sample size (n = 846,985) ensures that individual tree turnover has negligible impact on neighbourhood-level statistics.

3.2 Individual tree detection and quality filtering

Individual tree crowns were delineated via marker-controlled watershed segmentation of the inverted CHM, among the most widely benchmarked approaches for individual tree delineation from airborne LiDAR [44]. Local maxima (minimum height 2 m, minimum inter-peak distance 1.0 m) serve as markers, producing non-overlapping crown polygons suited to urban canopies where trees are often separated by streets and buildings [45], though the method systematically under-segments densely packed crowns (addressed in Dense Canopy Analysis below).

A seven-step quality filtering pipeline ensures label quality:

1. **Boundary clipping** to the municipality polygon (∼27% removal).
2. **Height capping** at 40 m (∼1% removal).
3. **Minimum crown area** of 8 m^2 (∼15% removal), optimized for 92% false-positive reduction at 8% true-positive cost.
4. **NDVI filtering** below 0.2 (∼5% removal).
5. **Spatial join with BOMEN register** at 5 m centroid distance (enrichment; no removal).
6. **Allometric flagging** of multi-tree suspects (flags only; see below).
7. **NMS deduplication** at IoU > 0.5 (∼3% removal).

Dense canopy analysis.

Watershed segmentation under-segments adjacent crowns when inter-tree saddle points are shallow. A two-tier approach quantifies rather than ignores this: Tier 1 flags polygons where observed crown diameter exceeds allometric expectations ($d_{\text{expected}} = 0.5 \cdot h^{0.8}$), and Tier 2 counts local maxima within each flagged polygon. Overall, 135,571 polygons (16.0%) are flagged: 48.9% confirmed single-tree, 46.5% likely multi-tree, 4.6% fragments. Flagged polygons are retained with diagnostic columns (Extended Data Fig. 3); recomputing key metrics after exclusion shifts mean LAI by <0.06 and neighbourhood rankings by Spearman $\rho = 0.988$.

3.3 Leaf Area Index extraction

LAI in this study represents effective plant area index ($\mathrm{PAI_e}$), derived from canopy gap fraction. AHN5-derived LAI rasters at 0.5 m resolution were sampled at each crown polygon centroid for every detected tree. Raster values are computed as:

$$\mathrm{LAI_{LiDAR}} = -\frac{\ln(P_{\mathrm{gap}})}{k_{\mathrm{LiDAR}}} \tag{1}$$

where P_{gap} is the canopy gap fraction and $k_{\mathrm{LiDAR}} = 0.3$ is the extinction coefficient for hemispherical canopy closure [26]. $\mathrm{PAI_e}$ includes woody elements (10–15% of total for broadleaf species in leaf-on condition [27, 30]). We use "LAI" as conventional shorthand for $\mathrm{PAI_e}$ throughout, following standard practice in urban LiDAR studies.

***k*-normalization for shade modeling.**

The Beer–Lambert inversion requires an extinction coefficient k that encodes the relationship between canopy geometry and radiation interception. For LiDAR gap-fraction retrieval, k depends on scanner viewing geometry; for shade modeling, k depends on the solar beam path. These are different quantities and must be distinguished [46].

Why $k_{LiDAR} = 0.3$. The AHN5 campaign employs near-nadir airborne laser scanning with scan angles typically $< 20°$ from vertical. At near-nadir incidence, the laser beam traverses the canopy primarily along the vertical axis, sampling projected foliage area from above. The effective extinction coefficient for this geometry is $k_{\mathrm{LiDAR}} = 0.3$, following the LiDAR gap-fraction retrieval framework of Richardson et al. [26].

Why $k_{solar} = 0.5$. Shade modeling requires transmissivity along the solar beam path, which traverses the canopy at oblique angles determined by solar elevation. The standard value $k_{\mathrm{solar}} = 0.5$ assumes spherical leaf angle distribution for broadleaf canopies [27]. This sits within the meta-analytic broadleaf range (mean $k = 0.59$) across 88 terrestrial ecosystems [47].

Why the normalization. Because LiDAR-derived $\mathrm{PAI_e}$ is calibrated to nadir viewing ($k_{\mathrm{LiDAR}} = 0.3$), using it directly with $k_{\mathrm{solar}} = 0.5$ would overestimate canopy opacity. The normalization

$$\begin{aligned} \mathrm{LAI_{solar}} &= K_{\mathrm{ratio}}\,\mathrm{LAI_{LiDAR}}, \qquad K_{\mathrm{ratio}} = \frac{k_{\mathrm{LiDAR}}}{k_{\mathrm{solar}}} = 0.6, \\ \tau &= \exp(-k_{\mathrm{solar}}\,\mathrm{LAI_{solar}})\,, \end{aligned} \tag{2}$$

separates the sensor-dependent retrieval from the application-dependent extinction [46]. Because $K_{\mathrm{ratio}} = k_{\mathrm{LiDAR}}/k_{\mathrm{solar}}$, this normalization makes τ reduce algebraically to the near-vertical LiDAR gap fraction P_{gap}; the reported τ is therefore best interpreted as a canopy-openness (gap-fraction) transmissivity rather than an independently calibrated oblique-beam value, and its comparison to uniform-model transmissivities is indicative. A physically resolved oblique solar-path transmissivity is left to future work.

Sensitivity bounds. The K coefficient affects absolute LAI magnitudes but not relative rankings: Almeida et al. demonstrated Spearman rank correlation of 1.0 across

pulse density classes and 0.95 across grain sizes $\leq$10 m in tropical broadleaf forest [27]. Varying the LAI-to-transmissivity conversion at fixed retrieved leaf area over $k \in [0.2, 0.6]$ moves citywide mean τ from 0.13 to 0.46, while genus-level rank correlation is preserved (Spearman $\rho = 0.976$); no genus lines cross across the full sweep. Urban trees with isolated, pruned crowns may exhibit different effective k due to non-random gap distributions [48], but this affects absolute magnitudes, not comparative rankings. Empirical k retrieval from multi-angular LiDAR [42] would bracket absolute values more tightly.

3.4 Effective Shade Area modeling

The ESA framework computes time-integrated, irradiance-weighted shadow footprints for each tree.

Solar geometry.

At each 30-minute time step between 09:00 and 17:00 local solar time (17 steps), solar azimuth and elevation are computed for Amsterdam on 3 August 2024 ($\gamma_{\max} = 56.8°$), the peak urban heat-island day in the RIVM record. Reporting is restricted to this single date to avoid relying on the constant-LAI assumption beyond the leaf-on summer window.

Shadow projection.

Each tree is modeled as an ellipsoidal crown at height $h_{\text{crown}} = h_{\text{tree}} - r_c$. The shadow centroid is displaced by $d = h_{\text{crown}} / \tan(\gamma)$; the footprint is an ellipse with $a = r_c / \sin(\gamma)$ and $b = r_c$.

Irradiance weighting and transmissivity.

Direct normal irradiance provides an irradiance weight w_t. Per-tree transmissivity τ_i modulates the effective shade:

$$\text{ESA}_{i,t} = A_{\text{shadow},i,t} \cdot (1 - \tau_i) \cdot w_t \tag{3}$$

Total per-tree ESA is the sum across time steps.

Building shadows and net tree shade.

Building shadows are computed from 3D BAG models using identical solar geometry. Net tree shade is defined as the tree shadow footprint minus its overlap with building shadows [15].

Sensitivity analysis.

A Monte Carlo simulation (n = 1,000 draws) simultaneously perturbs LAI ($\pm$20%), k ($\pm$20%), solar elevation ($\pm 2°$), and default transmissivity ($\pm$20%). The 90% confidence interval on citywide ESA is 0.49% of the mean, and neighbourhood Spearman rank correlation is $\rho = 0.9296 \pm 0.0009$ across all draws (Extended Data Fig. 2b).

Woody-fraction sensitivity.

The LiDAR-derived metric is effective plant area index ($\mathrm{PAI_e}$), which includes woody elements (bark, branches) in addition to leaves. To test whether the leaf-versus-plant distinction affects comparative conclusions, we apply a leaf-fraction scaling $\mathrm{LAI_{leaf}} = \alpha \cdot \mathrm{PAI_e}$ with $\alpha \in \{0.85, 0.90, 0.95, 1.00\}$, spanning the plausible range for broadleaf species in leaf-on condition, and recompute genus-mean transmissivity at each value. Genus rank order is invariant across all α (Spearman $\rho = 1.000$, Kendall $\tau = 1.000$; Extended Data Fig. 5). Absolute magnitudes scale with α: citywide mean genus τ increases from 0.288 at $\alpha = 1.00$ to 0.344 at $\alpha = 0.85$, corresponding to 2.88× and 3.44× the uniform $\tau = 0.10$ baseline respectively. The ∼3× ratio over uniform models is stable across any plausible leaf-fraction assumption, and no comparative conclusion in this paper depends on the choice of α.

Jensen gap analysis.

To quantify the shade contribution of within-neighbourhood LAI variance, for each neighbourhood with ≥50 trees ($n = 484$) we computed the empirical mean shade fraction $\overline{S}_{\mathrm{emp}} = \overline{1 - e^{-k\,\mathrm{LAI}_i}}$ (average across all trees in the neighbourhood) and the mean-aggregated prediction $S_{\mathrm{agg}} = 1 - e^{-k\,\overline{\mathrm{LAI}}}$ (shade computed from the neighbourhood mean LAI). The Jensen gap is $\Delta = \overline{S}_{\mathrm{emp}} - S_{\mathrm{agg}}$, expressed in percentage points. The second-order Taylor expansion of the concave function $f(x) = 1 - e^{-kx}$ around the neighbourhood mean predicts $\Delta_{\mathrm{theory}} = \frac{1}{2}k^2 e^{-k\mu}\,\mathrm{Var(LAI)}$; we compare empirical and theoretical gaps via linear regression across the 484 qualifying neighbourhoods.

3.5 Neighbourhood analysis and vulnerability index

Trees were spatially joined to the 519 CBS BUURT neighbourhoods: 516 contain at least one detected tree, 512 contain ≥50 trees, and 484 of those also meet the $\mathrm{CV} \geq 0.05$ within-neighbourhood variance threshold and qualify for the Jensen analysis. The Heat Vulnerability Index is reported for the 366 neighbourhoods with complete component data; the socioeconomic correlations use the 426 neighbourhoods with a non-suppressed mean housing value and the 452 with a computable bijstand rate (CBS suppresses income statistics at this level). Per-neighbourhood canopy cover is the ratio of total crown area to land area (excluding water). The Shade Gap Index quantifies per-neighbourhood shade deficit relative to the 30% canopy-cover benchmark of the 3-30-300 rule [9].

The Heat Vulnerability Index is a normalized composite of three equally weighted components, each min-max scaled to [0, 1]: UHI exposure (RIVM, 10 m), canopy deficit (inverse ESA-derived shade supply), and elderly population share (% aged 65+, CBS 2023). Because the socioeconomic and health components of a full vulnerability index [32] are suppressed at this resolution, this composite is an exposure-plus-age screen rather than a complete vulnerability measure. The 73 neighbourhoods in its top quintile serve as an indicative screen for prioritisation, not a definitive ranking.

3.6 PAI_e consistency assessment

Three independent tests confirm that relative rankings are stable under parameter uncertainty. First, the extinction-coefficient sweep ($k_{\mathrm{LiDAR}} \in [0.2, 0.6]$) preserves genus-level transmissivity rank at Spearman $\rho = 0.976$ with no genus lines crossing. Second, Monte Carlo sensitivity ($n = 1{,}000$ draws with $\pm 20\%$ simultaneous perturbation of LAI, k, solar elevation, and default τ) yields a 90% confidence interval width of 0.49% of mean ESA and neighbourhood rank $\rho = 0.9296 \pm 0.0009$. Third, woody-fraction correction ($\alpha \in \{0.85, 0.90, 0.95, 1.00\}$) leaves genus rank invariant ($\rho = 1.000$ at all α; Extended Data Fig. 5). Propagating the LiDAR and solar extinction coefficients and the woody fraction *jointly* (credible priors $k_{\mathrm{LiDAR}} \in [0.25, 0.40]$, $\alpha \in [0.85, 1.0]$; k_{solar} cancels in the normalization) bounds the citywide per-tree transmissivity at $\approx$2.2–4.3$\times$ the uniform $\tau = 0.10$ (central $\approx$3.1$\times$), with k_{LiDAR} the dominant source of spread. Excluding all 135,571 flagged multi-tree polygons shifts mean LAI by $<$0.06 and neighbourhood rankings by $\rho = 0.988$ (Extended Data Fig. 3). Recomputing the Jensen gap on the 701,192 unflagged trees alone leaves it essentially unchanged (mean +2.74 pp vs +2.84 pp; $R^2 = 0.987$; $n = 482$), confirming that crown under-segmentation does not materially inflate or deflate the within-neighbourhood variance term.

Raster-derived PAI_e values are systematically lower than published species-specific references by $\sim$2.4 units across all genera examined (Extended Data Fig. 2a). The offset is approximately additive (constant across genera and tree sizes) rather than multiplicative, which preserves genus rank order regardless of the absolute calibration level. Because an additive LAI offset shifts every genus-mean transmissivity by a common multiplicative factor, it leaves the *ratios* between genera unchanged: the observed 1.3-fold genus range is therefore a property of the measured canopy, not an artifact of the offset. That this range is far narrower than the $\sim$7-fold span reported for unconstrained single-tree specimens [22] is itself substantive: urban growing conditions (pruning, restricted rooting volume, competition for light) homogenize crown density across genera relative to forest-grown trees, so species selection operates over a real but compressed range. This offset is expected: literature values represent isolated, fully foliated specimens, whereas LiDAR-derived PAI_e captures actual canopy conditions including gaps and urban growing constraints. Five Ulmus trees measured via hemispherical photography (RMSE = 0.86 m^2/m^2 versus LiDAR estimates) confirm physical plausibility; this discrepancy lies within the inter-method variability (CV $>$ 30%) documented for hemispherical photography of isolated urban trees [41]. This spot-check is limited to a single genus and season; dedicated field campaigns remain a priority.

Absolute PAI_e magnitudes and derived transmissivity values should be interpreted as bounded estimates pending dedicated field validation; the comparative rankings that drive this paper's conclusions are stable across all parameter perturbations examined.

Acknowledgements This work used the MIT ORCD HPC cluster for computational processing. The AHN5 LiDAR data were provided by the Dutch Kadaster. CBS neighborhood boundary data were obtained from Statistics Netherlands.

Declarations **Funding** This research was supported by the Senseable City Lab Consortium at MIT.

Competing Interests The authors declare no competing interests.

Data Availability The complete Amsterdam per-tree urban-forest dataset will be released publicly on Hugging Face at https://huggingface.co/datasets/thrmnn/invisible-forest-amsterdam upon peer-reviewed publication; a preprint of this manuscript is posted on EarthArXiv. The analysis draws on the following public inputs: the Amsterdam BOMEN municipal tree register (2026 release), AHN5 national LiDAR and PDOK DSM/DTM (Kadaster/PDOK), Kadaster aerial RGB and colour-infrared imagery, CBS neighbourhood boundaries and demographics, RIVM urban-heat-island data, and 3D BAG LOD2 building models.

Code Availability The full processing pipeline and trained models will be released at https://github.com/thrmnn/invisible-forest upon peer-reviewed publication; documentation is available there now.

Author Contributions T.H. conceived the study, developed the methodology, performed all analyses, wrote the original draft, and created all visualizations. M.v.S. contributed to the investigation and provided writing, review & editing. T.V. supervised the research locally and provided resources, facilitating data access at the Amsterdam Institute for Advanced Metropolitan Solutions. F.D. contributed to conceptualization and supervision, and provided writing, review & editing. C.R. provided supervision, resources, funding acquisition, and project administration. All authors reviewed and approved the final manuscript.

References

[1] Turner, V.K., Middel, A., Vanos, J.K.: Shade is an essential solution for hotter cities. Nature **619**, 694–697 (2023) https://doi.org/10.1038/d41586-023-02311-3

[2] Middel, A., Selover, N., Hagen, B., Chhetri, N.: Impact of shade on outdoor thermal comfort-a seasonal field study in Tempe, Arizona. International Journal of Biometeorology **60**(12), 1849–1861 (2016) https://doi.org/10.1007/s00484-016-1172-5

[3] Rahman, M.A., Stratopoulos, L.M.F., Moser-Reischl, A., Zölch, T., Häberle, K.-H., Rötzer, T., Pretzsch, H., Pauleit, S.: Traits of trees for cooling urban heat islands: A meta-analysis. Building and Environment **170**, 106606 (2020) https://doi.org/10.1016/j.buildenv.2019.106606

[4] Schwaab, J., Meier, R., Mussetti, G., Seneviratne, S., Bürgi, C., Davin, E.L.: The role of urban trees in reducing land surface temperatures in European cities. Nature Communications **12**, 6763 (2021) https://doi.org/10.1038/s41467-021-26768-w

[5] Gillner, S., Vogt, J., Tharang, A., Dettmann, S., Roloff, A.: Role of street trees in mitigating effects of heat and drought at highly sealed urban sites. Landscape and Urban Planning **143**, 33–42 (2015) https://doi.org/10.1016/j.landurbplan.

2015.06.005

[6] Armson, D., Stringer, P., Ennos, A.R.: The effect of tree shade and grass on surface and globe temperatures in an urban area. Urban Forestry & Urban Greening **11**, 245–255 (2012) https://doi.org/10.1016/j.ufug.2012.05.002

[7] Heaviside, C., Macintyre, H., Vardoulakis, S.: The Urban Heat Island: Implications for Health in a Changing Environment. Current Environmental Health Reports **4**(3), 296–305 (2017) https://doi.org/10.1007/s40572-017-0150-3

[8] World Health Organization: Urban green spaces and health: A review of evidence. Technical report, WHO Regional Office for Europe, Copenhagen (2016)

[9] Konijnendijk, C.C.: Evidence-based guidelines for greener, healthier, more resilient neighbourhoods: Introducing the 3–30–300 rule. Journal of Forestry Research **34**, 821–830 (2023) https://doi.org/10.1007/s11676-022-01523-z

[10] European Parliament and Council: Regulation (EU) 2024/1991 of the European Parliament and of the Council on Nature Restoration. Official Journal of the European Union L 2024/1991. Article 8: Urban ecosystems (2024)

[11] Schwarz, K., Fragkias, M., Boone, C.G., Zhou, W., McHale, M., Grove, J.M., O'Neil-Dunne, J., McFadden, J.P., Buckley, G.L., Childers, D., Ogden, L., Pincetl, S., Pataki, D., Whitmer, A., Cadenasso, M.L.: Trees grow on money: Urban tree canopy cover and environmental justice. PLOS ONE **10**, 0122051 (2015) https://doi.org/10.1371/journal.pone.0122051

[12] Harlan, S.L., Brazel, A.J., Prashad, L., Stefanov, W.L., Larsen, L.: Neighborhood microclimates and vulnerability to heat stress. Social Science & Medicine **63**, 2847–2863 (2006) https://doi.org/10.1016/j.socscimed.2006.07.030

[13] Schlosberg, D.: Defining Environmental Justice: Theories, Movements, and Nature. Oxford University Press, Oxford (2007)

[14] Gu, X., Beuster, L., Liu, X., Leeuwen, E., Venverloo, T., Duarte, F.: Global patterns of inequality in pedestrian shade provision. Nature Communications **17**, 2563 (2026) https://doi.org/10.1038/s41467-026-69190-w

[15] Beuster, L., Selm, M., Venverloo, T., García-Sánchez, C., Duarte, F., Ledoux, H.: (slim) shady—the relative role of buildings and trees in urban shade provision for pedestrians. Preprint at Research Square (2025) https://doi.org/10.21203/rs.3.rs-6966874/v1

[16] Lindberg, F., Holmer, B., Thorsson, S.: SOLWEIG 1.0 – modelling spatial variations of 3D radiant fluxes and mean radiant temperature in complex urban settings. International Journal of Biometeorology **52**(7), 697–713 (2008) https://doi.org/10.1007/s00484-008-0162-7

[17] Östberg, J., Wiström, B., Randrup, T.B.: The state and use of municipal tree inventories in Swedish municipalities. Urban Ecosystems **21**(3), 467–477 (2018) https://doi.org/10.1007/s11252-018-0732-3

[18] Ordóñez, C., Duinker, P.N.: An analysis of urban forest management plans in Canada: Implications for urban forest management. Landscape and Urban Planning **116**, 36–47 (2013) https://doi.org/10.1016/j.landurbplan.2013.04.007

[19] Nowak, D.J., Greenfield, E.J.: US Urban Forest Statistics, Values, and Projections. Journal of Forestry **116**(2), 164–177 (2018) https://doi.org/10.1093/jofore/fvx004

[20] Thomas, N., Baltezar, P., Lagomasino, D., Stovall, A., Iqbal, Z., Fatoyinbo, L.: Trees outside forests are an underestimated resource in a country with low forest cover. Scientific Reports **11**(1), 7919 (2021) https://doi.org/10.1038/s41598-021-86944-2

[21] Chen, J.M., Black, T.A.: Defining leaf area index for non-flat leaves. Plant, Cell & Environment **15**(4), 421–429 (1992) https://doi.org/10.1111/j.1365-3040.1992.tb00992.x

[22] Konarska, J., Lindberg, F., Larsson, A., Thorsson, S., Holmer, B.: Transmissivity of solar radiation through crowns of single urban trees—application for outdoor thermal comfort modelling. Theoretical and Applied Climatology **117**(3–4), 363–376 (2014) https://doi.org/10.1007/s00704-013-1000-3

[23] Sjöman, H., Östberg, J., Bühler, O.: Diversity and distribution of the urban tree population in ten major Nordic cities. Urban Forestry & Urban Greening **11**, 31–39 (2012) https://doi.org/10.1016/j.ufug.2011.09.004

[24] Nielsen, A.B., Bosch, M., Maruthaveeran, S., Bosch, C.K.: Species richness in urban parks and its drivers: A review of empirical evidence. Urban Ecosystems **17**, 305–327 (2014) https://doi.org/10.1007/s11252-013-0316-1

[25] Foresta, H., Somarriba, E., Temu, A., Boulanger, D., Feuilly, H., Gauthier, M.: Towards the assessment of trees outside forests. Resources Assessment Working Paper **183** (2013)

[26] Richardson, J.J., Moskal, L.M., Kim, S.-H.: Modeling approaches to estimate effective leaf area index from aerial discrete-return LiDAR. Agricultural and Forest Meteorology **149**(6–7), 1152–1160 (2009) https://doi.org/10.1016/j.agrformet.2009.02.007

[27] Almeida, D.R.A.d., Stark, S.C., Chazdon, R., Nelson, B.W., Cesar, R.G., Meli, P., Gorgens, E.B., Duarte, M.M., Valbuena, R., Moreno, V.S., Mendes, A.F., Amazonas, N., Gonçalves, N.B., Silva, C.A., Schietti, J., Brancalion, P.H.S.: The effectiveness of lidar remote sensing for monitoring forest cover attributes and

landscape restoration. Forest Ecology and Management **438**, 34–43 (2019) https://doi.org/10.1016/j.foreco.2019.02.002

[28] Kissling, W.D., Shi, Y., Koma, Z., Meijer, C., Ku, O., Nattino, F., Seijmonsbergen, A.C., Grootes, M.W.: Country-wide data of ecosystem structure from the third Dutch airborne laser scanning survey. Data in Brief **46**, 108798 (2023) https://doi.org/10.1016/j.dib.2022.108798

[29] Klingberg, J., Konarska, J., Lindberg, F., Johansson, L., Thorsson, S.: Mapping leaf area of urban greenery using aerial LiDAR and ground-based measurements in Gothenburg, Sweden. Urban Forestry & Urban Greening **26**, 31–40 (2017) https://doi.org/10.1016/j.ufug.2017.05.011

[30] Fang, H., Baret, F., Plummer, S., Schaepman-Strub, G.: An overview of global leaf area index (LAI): Methods, products, validation, and applications. Reviews of Geophysics **57**, 739–799 (2019) https://doi.org/10.1029/2018RG000608

[31] Croeser, T., Sharma, R., Weisser, W.W., Bekessy, S.A.: Acute canopy deficits in global cities exposed by the 3–30–300 benchmark for urban nature. Nature Communications **15**, 9333 (2024) https://doi.org/10.1038/s41467-024-53402-2

[32] Reid, C.E., O'Neill, M.S., Gronlund, C.J., Brines, S.J., Brown, D.G., Diez-Roux, A.V., Schwartz, J.: Mapping community determinants of heat vulnerability. Environmental Health Perspectives **117**, 1730–1736 (2009) https://doi.org/10.1289/ehp.0900683

[33] Randrup, T.B., Persson, B.: Public green spaces in the Nordic countries: Development of a new strategic management regime. Urban Forestry & Urban Greening **8**, 31–40 (2009) https://doi.org/10.1016/j.ufug.2008.08.004

[34] Gemeente Amsterdam: Bomenverordening 2014 (Tree Ordinance). Technical report, Gemeente Amsterdam, Amsterdam (2016)

[35] Galle, N.: Amsterdam's Urban Forest is Disappearing Due to Private Tree Removal Permits. Het Parool. Analysis of Amsterdam tree felling permit data, 2022–2023. https://www.nadinagalle.com/blog/opinion-our-urban-forest-is-vanishing--how-private-tree-removal-permits-are-accelerating-its-decline (2025)

[36] Gemeente Amsterdam: Groenvisie 2050: Een groener Amsterdam. Technical report, Gemeente Amsterdam, Amsterdam (2020)

[37] Klaus, V.H., Řehounková, K., Valkó, O., Degtjarenko, P., Schelfhout, S.: Countries need ambitious urban biodiversity targets under the EU Nature Restoration Law. npj Urban Sustainability **5**(1), 22 (2025) https://doi.org/10.1038/s42949-025-00218-8

[38] Gould, K.A., Lewis, T.L.: Green Gentrification: Urban Sustainability and the

Struggle for Environmental Justice. Routledge, London (2017)

[39] Anguelovski, I., Connolly, J.J.T., Garcia-Lamarca, M., Cole, H., Pearsall, H.: New scholarly pathways on green gentrification: What does the urban 'green turn' mean and where is it going? Progress in Human Geography **43**(6), 1064–1086 (2019) https://doi.org/10.1177/0309132518803799

[40] Pellerey, V., Giezen, M.: More green but less just? Analyzing urban green spaces, participation, and environmental justice in Amsterdam. Journal of Environmental Planning and Management **69**(3), 855–889 (2024) https://doi.org/10.1080/09640568.2024.2406858

[41] Peper, P.J., McPherson, E.G.: Comparison of five methods for estimating leaf area index of open-grown deciduous trees. Arboriculture & Urban Forestry **24**(2), 98–111 (1998) https://doi.org/10.48044/jauf.1998.013

[42] Ma, L., Zheng, G., Eitel, J.U.H., Magney, T.S., Moskal, L.M.: Retrieving forest canopy extinction coefficient from terrestrial and airborne LiDAR. Agricultural and Forest Meteorology **236**, 1–21 (2017) https://doi.org/10.1016/j.agrformet.2017.01.004

[43] Konarska, J., Uddling, J., Holmer, B., Lutz, M., Lindberg, F., Pleijel, H., Thorsson, S.: Transpiration of urban trees and its cooling effect in a high latitude city. International Journal of Biometeorology **60**, 159–172 (2016) https://doi.org/10.1007/s00484-015-1014-x

[44] Kaartinen, H., Hyyppä, J., Yu, X., Vastaranta, M., Hyyppä, H., Kukko, A., Holopainen, M., Heipke, C., Hirschmugl, M., Morsdorf, F., Næsset, E., Pitkänen, J., Popescu, S., Solberg, S., Wolf, B.M., Wu, J.-C.: An international comparison of individual tree detection and extraction using airborne laser scanning. Remote Sensing **4**(4), 950–974 (2012) https://doi.org/10.3390/rs4040950

[45] Fassnacht, F.E., Latifi, H., Stereńczak, K., Modzelewska, A., Lefsky, M., Waser, L.T., Straub, C., Ghosh, A.: Review of studies on tree species classification from remotely sensed data. Remote Sensing of Environment **186**, 64–87 (2016) https://doi.org/10.1016/j.rse.2016.08.013

[46] Jonckheere, I., Fleck, S., Nackaerts, K., Muys, B., Coppin, P., Weiss, M., Baret, F.: Review of methods for in situ leaf area index determination: Part I. theories, sensors and hemispherical photography. Agricultural and Forest Meteorology **121**(1–2), 19–35 (2004) https://doi.org/10.1016/j.agrformet.2003.08.027

[47] Zhang, L., Hu, Z., Fan, J., Zhou, D., Tang, F.: A meta-analysis of the canopy light extinction coefficient in terrestrial ecosystems. Frontiers of Earth Science **8**(4), 599–609 (2014) https://doi.org/10.1007/s11707-014-0446-7

[48] Kamoske, A.G., Dahlin, K.M., Stark, S.C., Serbin, S.P.: Leaf area density from

airborne LiDAR: Comparing sensors and resolutions in a temperate broadleaf forest ecosystem. Forest Ecology and Management **433**, 364–375 (2019) https://doi.org/10.1016/j.foreco.2018.11.017

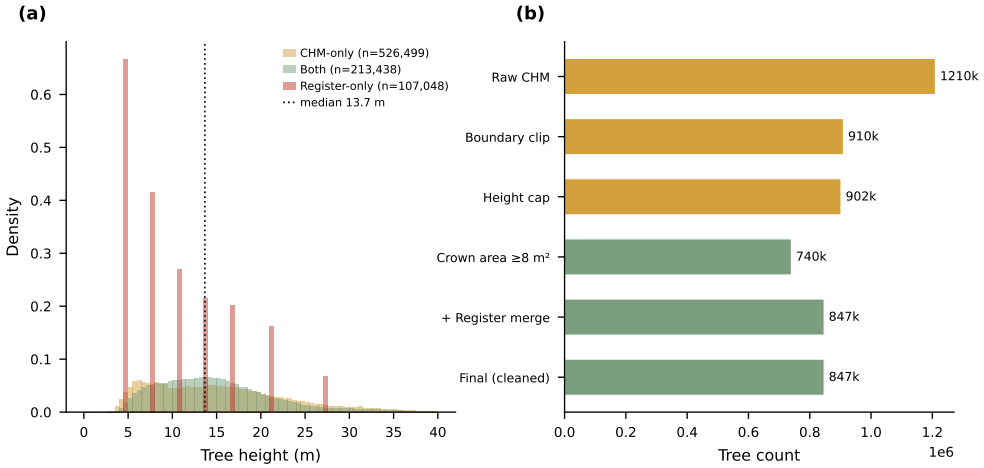

Extended Data Fig. 1: **Tree detection pipeline and canopy height. a,** Height distribution by source: CHM-only (n = 526,499), both sources (n = 213,438), and register-only (n = 107,048). Median height 13.7 m. **b,** Detection pipeline yield from ∼1.21 M raw CHM detections to 846,985 merged labels after BOMEN 2026 re-join.

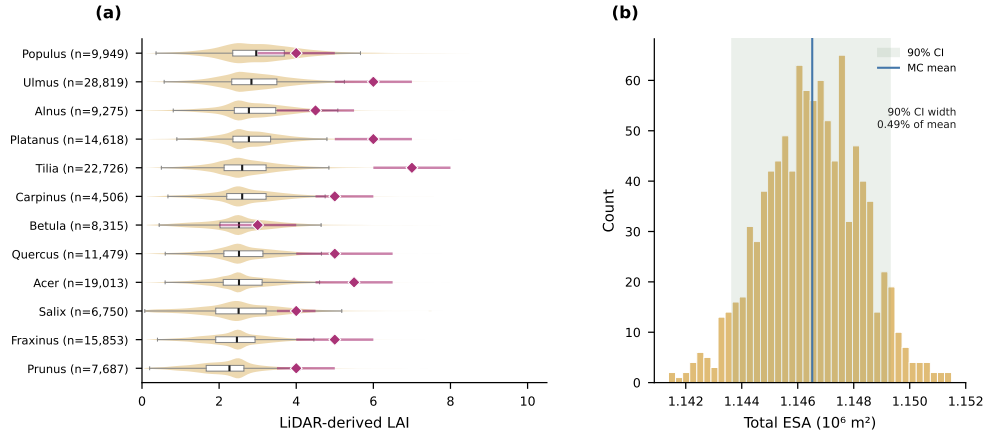

Extended Data Fig. 2: **LAI validation suite. a,** Species-specific LAI distributions from LiDAR raster extraction (violin plots, per-genus n shown) compared with published reference values (diamonds) for 12 genera. A consistent offset of $\sim$2.4 units reflects the difference between effective $\mathrm{PAI_e}$ and literature LAI; the offset is approximately additive (constant across genera) rather than multiplicative, preserving genus rank order regardless of absolute calibration. **b,** Monte Carlo sensitivity: distribution of citywide total ESA across 1,000 joint-perturbation draws, with a 90% confidence-interval width of 0.49% of the mean.

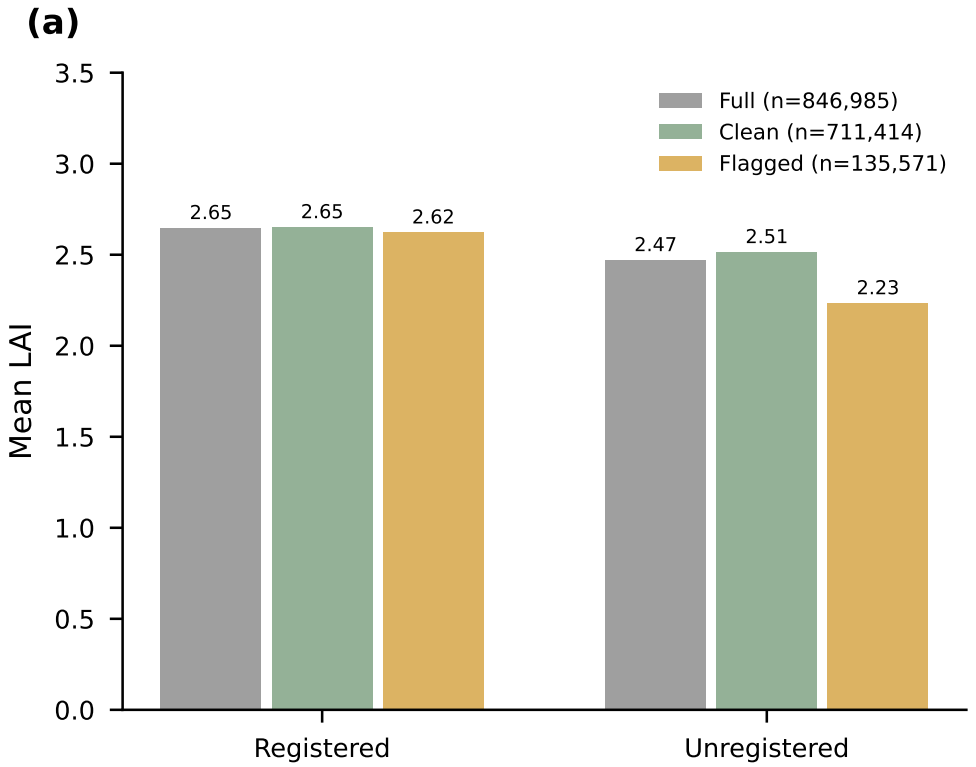

Extended Data Fig. 3: **Multi-tree polygon sensitivity.** Mean LAI by registration status: the full inventory versus excluding the 135,571 flagged multi-tree polygons. Mean LAI shifts <0.06 and neighbourhood rankings by Spearman $\rho = 0.988$.

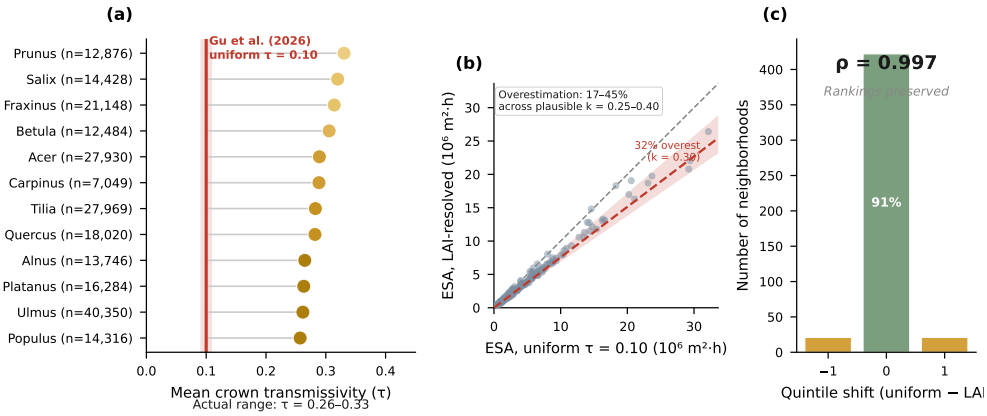

Extended Data Fig. 4: **Uniform vs per-tree shade.** Neighbourhood ESA under uniform $\tau = 0.10$ vs LAI-resolved τ: uniform model overestimates shade by ∼21% ($\rho = 0.997$, 91% same quintile). k-sweep uncertainty band spans 17–45% overestimation.

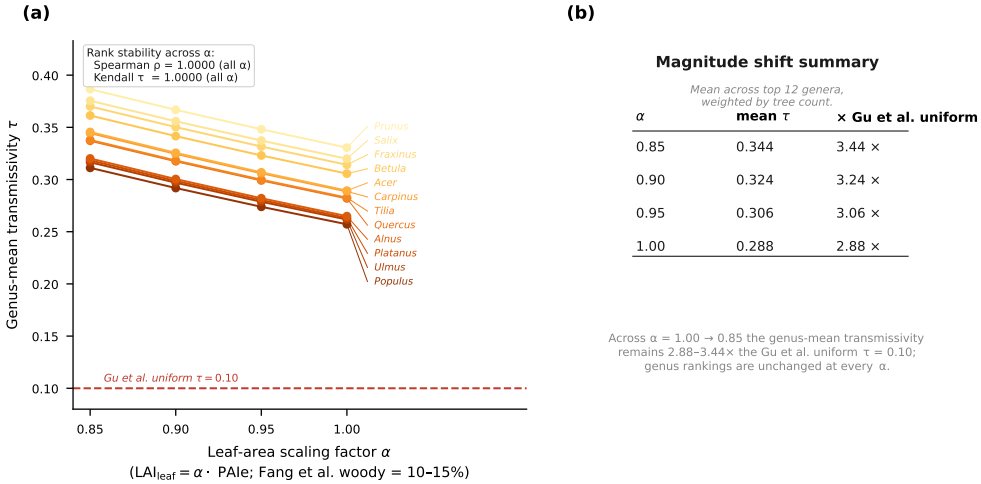

Extended Data Fig. 5: Woody-fraction sensitivity. $\mathrm{PAI_e}$ scaled by $\alpha \in \{0.85, 0.90, 0.95, 1.00\}$: genus rank invariant ($\rho = 1.000$ at all α). Magnitude shifts $2.88\times$ ($\alpha = 1.00$) to $3.44\times$ ($\alpha = 0.85$) relative to uniform $\tau = 0.10$.

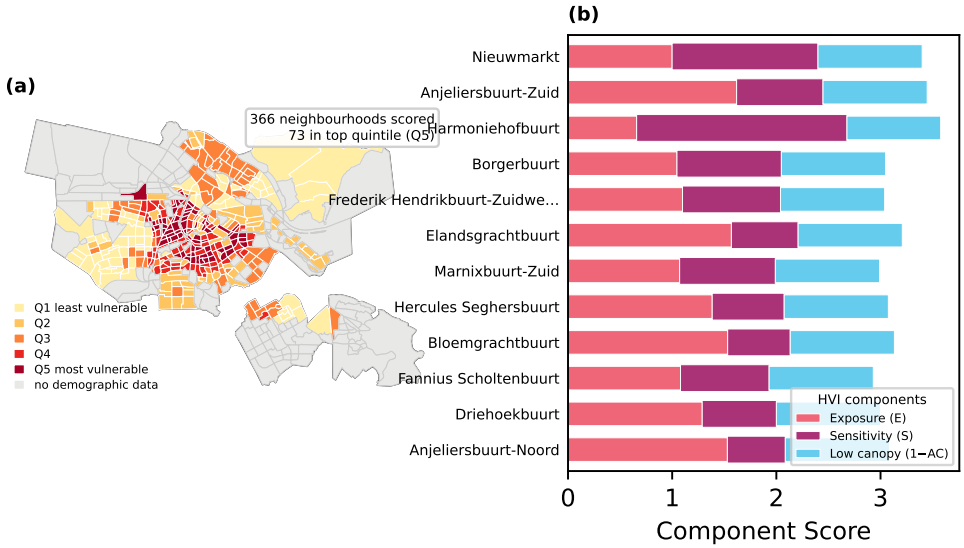

Extended Data Fig. 6: **Heat Vulnerability Index. a,** HVI quintiles across the 366 neighbourhoods with complete demographic data; the 153 without CBS demographics are shown in grey. **b,** The twelve highest-HVI neighbourhoods, decomposed into exposure, sensitivity, and low-canopy components. HVI sums three equally weighted components, each min-max scaled to [0, 1] (UHI exposure, canopy deficit, elderly population share). The top three (Nieuwmarkt = 1.40, Anjeliersbuurt-Zuid 1.34, Harmoniehofbuurt 1.20) are stable across alternative weighting schemes (Spearman $\rho = 0.74$); the full top-quintile list (73 neighbourhoods) is indicative screening, not a definitive ranking. The canopy-deficit component derives from the shadow-modelled shade layer, which is comparative and will be refreshed against the full canopy inventory in revision.

Supplementary Information

Per-tree leaf area index mapping of Amsterdam's unrecorded shade canopy

Théo Alessandro Hermann, Michiel van Selm, Titus Venverloo, Fabio Duarte, Carlo Ratti

S1 PAI_e vs LAI: Terminology and Implications

The LiDAR-derived values reported in this study represent effective plant area index (PAI_e), not classical leaf-only LAI. PAI_e includes all canopy elements intercepting LiDAR pulses: leaves, bark, branches, and epiphytes. For broadleaf species in full leaf-on condition (as captured by the AHN5 summer acquisitions), woody elements typically contribute 10–15% of total PAI_e [1].

For the shade modeling application in this study, PAI_e is arguably more appropriate than classical LAI: radiation interception depends on all canopy elements encountered along the beam path, not only leaves. The Beer-Lambert transmissivity $\tau = \exp(-k \cdot \mathrm{PAI_e})$ therefore captures the actual radiation attenuation more faithfully than a leaf-only metric would. The consistent 2.4-unit offset between our raster-derived values and published species-specific LAI references (Extended Data Fig. 2a) is largely attributable to this distinction, plus the difference between field-measured maximum LAI (isolated, fully foliated specimens) and LiDAR-observed effective PAI_e (actual urban canopy conditions with gaps, asymmetry, and management effects).

Throughout the main text, we use "LAI" as the conventional shorthand, noting the PAI_e distinction in the Methods and here.

S2 Quality Filtering Pipeline

Supplementary Table S1 details the seven-step quality filtering pipeline applied to watershed-segmented crown polygons. Steps are ordered for computational efficiency: inexpensive geometric filters precede raster-based operations. The pipeline was developed iteratively using BOMEN register matches as ground truth for false-positive assessment.

The $8\,\mathrm{m}^2$ minimum crown area threshold (Step 3) was selected by evaluating the trade-off between false-positive removal and true-positive retention across the range 4–$20\,\mathrm{m}^2$, using BOMEN register matches (5 m centroid distance) as positive labels. At $8\,\mathrm{m}^2$, the filter achieves 92% reduction in false positives (non-vegetated small polygons) at 8% cost to true positives (legitimate small trees). The threshold preferentially removes rooftop features, antenna bases, and segmentation fragments while retaining the vast majority of actual tree crowns.

S3 Dense Canopy Analysis

Watershed segmentation produces a single polygon for adjacent crowns when the inter-tree saddle point in the CHM is shallow relative to the canopy peaks. This under-segmentation is not random: it concentrates in parks, dense residential gardens, and canal-side corridors, precisely where unregistered trees cluster and where accurate shade accounting is most important.

The two-tier flagging system quantifies this issue without discarding data:

Table S1: Seven-step quality filtering pipeline. Removal percentages are cumulative from the raw segmentation output.

Step	Filter	Purpose	Parameter	Removal (%)
1	Boundary clip	Remove out-of-municipality detections	Amsterdam polygon	∼27
2	Height cap	Remove non-tree artifacts (cranes, LiDAR errors)	40 m	∼1
3	Crown area	Remove sub-tree fragments	8 m^2 min	∼15
4	NDVI filter	Remove non-vegetated elevated features	NDVI < 0.2	∼5
5	Register join	Enrich with species, height, planting year	5 m match	0 (enrichment)
6	Allometric flag	Identify potential multi-tree merges	See §S3	0 (flag only)
7	NMS dedup	Remove tile-boundary duplicates	IoU > 0.5	∼3

Tier 1 (Allometric anomaly detection) flags polygons where observed crown dimensions exceed allometric expectations. Expected crown diameter is modelled as $d_{\text{expected}} = 0.5 \cdot h^{0.8}$, following established urban tree allometric relationships. A polygon is flagged if any condition is met: (a) observed diameter $> 2 \times d_{\text{expected}}$, (b) circularity < 0.2 and area $> 50\,m^2$, or (c) elongation > 0.75 and area $> 50\,m^2$.

Tier 2 (Local maxima counting) performs CHM peak detection within each flagged polygon (minimum inter-peak distance: 1.0 m). Polygons with $n_{\text{peaks}} \geq 2$ are classified as likely multi-tree merges. The resulting classification: 48.9% confirmed single-tree, 46.5% likely multi-tree, 4.6% fragments. Supplementary Figure S2 shows representative examples, the classification distribution, and the spatial concentration of flagged polygons in parks and gardens.

All 135,571 flagged polygons (16.0% of the database) are retained with diagnostic columns (allometric ratio, circularity, elongation, peak count, estimated tree count), enabling users to apply custom filtering thresholds for their specific applications.

S4 Species LAI Reference Values

Table S2: Genus-specific LAI reference values used for the 3.4% of trees that carry a species label but no LiDAR raster coverage (a subset of the 12.6% gap-filled fraction). Values represent published leaf-on maxima for mature urban specimens.

Genus	Reference LAI (m^2/m^2)	Primary Source
Tilia	7.0	Konarska et al. 2014
Platanus	6.0	Peper et al. 2001
Quercus	5.5	Breuer et al. 2003
Acer	5.0	Breuer et al. 2003
Ulmus	5.0	Nowak 1996
Broadleaf default	5.0	Multi-source
Fraxinus	4.0	Breuer et al. 2003
Betula	3.5	Konarska et al. 2014

These values represent published maxima for isolated, fully foliated, mature specimens and are systematically higher than the LiDAR-derived PAI_e values (mean offset ∼2.4 units; see Extended Data Fig. 2a and §S1). The consistent cross-genus offset supports the use of these literature values as an upper-bound tier for trees lacking raster coverage, while the LiDAR-derived values reflect actual in-situ canopy conditions.

S5 Effective Shade Area: Extended Methodology

Shadow geometry derivation

At each time step t, the solar position is defined by azimuth α_t (compass bearing of the sun) and elevation γ_t (angle above the horizon). For a tree modelled as an ellipsoidal crown of radius r_c centred at height h_{crown}:

- **Shadow displacement**: The shadow centroid is offset from the trunk base by distance $d_t = h_{\text{crown}}/\tan(\gamma_t)$ in the direction $\alpha_t + 180°$.
- **Shadow elongation**: The shadow footprint is an ellipse with semi-major axis $a_t = r_c/\sin(\gamma_t)$ (elongated along the solar bearing) and semi-minor axis $b_t = r_c$ (perpendicular).
- **Shadow area**: $A_{\text{shadow},t} = \pi \cdot a_t \cdot b_t = \pi r_c^2/\sin(\gamma_t)$.

At low solar elevations ($\gamma < 15°$), shadows become unrealistically elongated. We apply a solar elevation floor of $\gamma_{\min} = 10°$ to avoid numerical instabilities; time steps with $\gamma < \gamma_{\min}$ are excluded from the integration.

Irradiance weighting

Direct normal irradiance I_t is estimated from solar elevation via a simplified clear-sky atmospheric model:

$$I_t = I_0 \cdot \exp\left(-\frac{0.14}{\sin(\gamma_t)}\right)$$

where $I_0 = 1361\,\text{W/m}^2$ is the solar constant. The irradiance weight $w_t = I_t/\sum_t I_t$ normalizes contributions across time steps, ensuring that midday shadows (high irradiance) contribute more to the integrated ESA than early-morning or late-afternoon shadows.

Per-tree ESA integration

The Effective Shade Area for tree i on a given date is:

$$\text{ESA}_i = \sum_{t=1}^{T} A_{\text{shadow},i,t} \cdot (1 - \tau_i) \cdot w_t \cdot \Delta t$$

where $T = 17$ time steps (09:00–17:00 at 30-minute intervals), τ_i is the per-tree transmissivity from Equation 2 in the main text, and $\Delta t = 0.5\,\text{h}$. The units are $\text{m}^2\,\text{h}$: irradiance-weighted shade area accumulated over the diurnal cycle.

Protection gap: top-decile shade trees by registration

Ranking trees by gross ESA and cross-referencing registration status maps the neighbourhoods where the highest-shade trees are the least protected (main text Fig. 4b). Because this ranking is computed on the shadow-modelled tree set, which predates the final register re-join, the per-neighbourhood top-decile splits are reported comparatively rather than as absolute counts, and will be refreshed against the full canopy inventory in revision.

S6 Sensitivity Analysis

One-at-a-time perturbation

Each parameter is independently varied by $\pm 20\%$ from its baseline value while holding all others constant. The resulting change in citywide ESA is expressed as a percentage of the baseline, producing a tornado chart that ranks parameters by influence.

Monte Carlo joint perturbation

All parameters are simultaneously drawn from independent uniform distributions: $k_{\text{solar}} \sim U(0.4, 0.6)$, LAI scaling factor $\sim U(0.8, 1.2)$, solar elevation offset $\sim U(-2°, +2°)$, default transmissivity $\sim U(0.08, 0.12)$. For each of $n = 1{,}000$ draws, the full ESA computation is repeated and neighborhood-level shade rankings are compared to the baseline via Spearman ρ.

The 90% confidence interval on citywide ESA is 0.49% of the baseline mean. Neighborhood rank correlation exceeds $\rho = 0.93$ across all draws, confirming that the comparative findings central to the policy recommendations are robust to the joint parameter uncertainties considered.

The figures below document validation and quality-control procedures referenced in the main text: hemispherical-photography validation of the LiDAR-derived LAI on five Ulmus trees (Supplementary Fig. S1, Table S3).

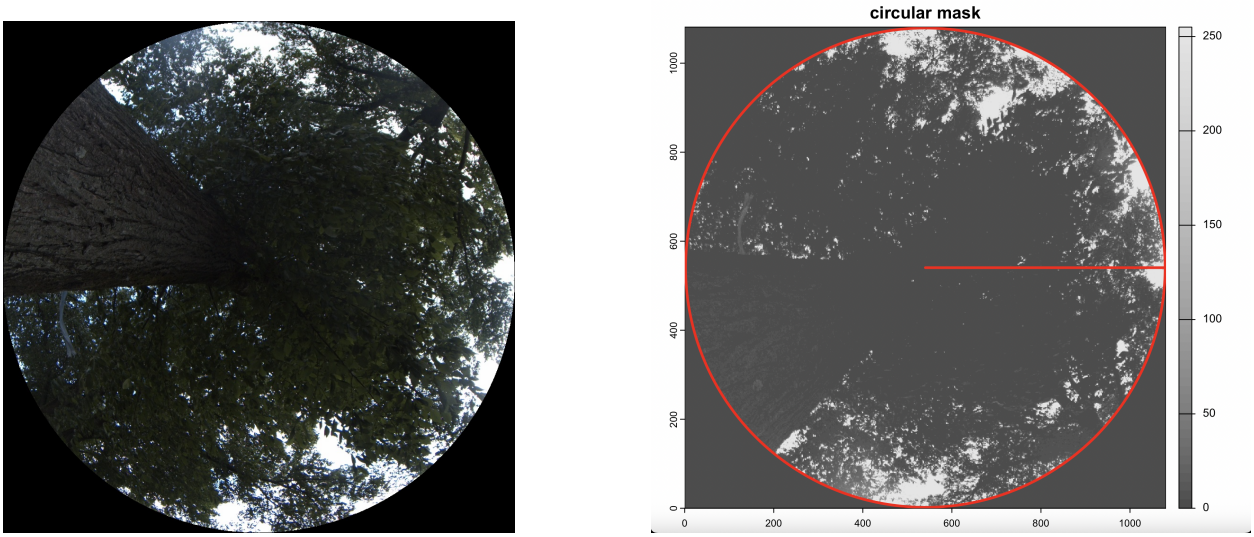

(a) Original hemispherical image

(b) Binarized for gap fraction

Figure S1: **Hemispherical photography validation.** (a) Upward-looking hemispherical fisheye image capturing canopy gap structure beneath an Ulmus tree. (b) Binarized image for gap fraction analysis. Five Ulmus trees measured via this method produced LAI values of 1.98–6.70 m^2/m^2 (RMSE = 0.86 vs LiDAR-derived estimates), confirming physical plausibility.

Table S3: Hemispherical photography LAI measurements for five Ulmus trees in Amsterdam.

Tree ID	Genus	Effective LAI (m^2/m^2)
1	Ulmus	6.70
2	Ulmus	4.33
3	Ulmus	3.19
4	Ulmus	2.92
5	Ulmus	1.98

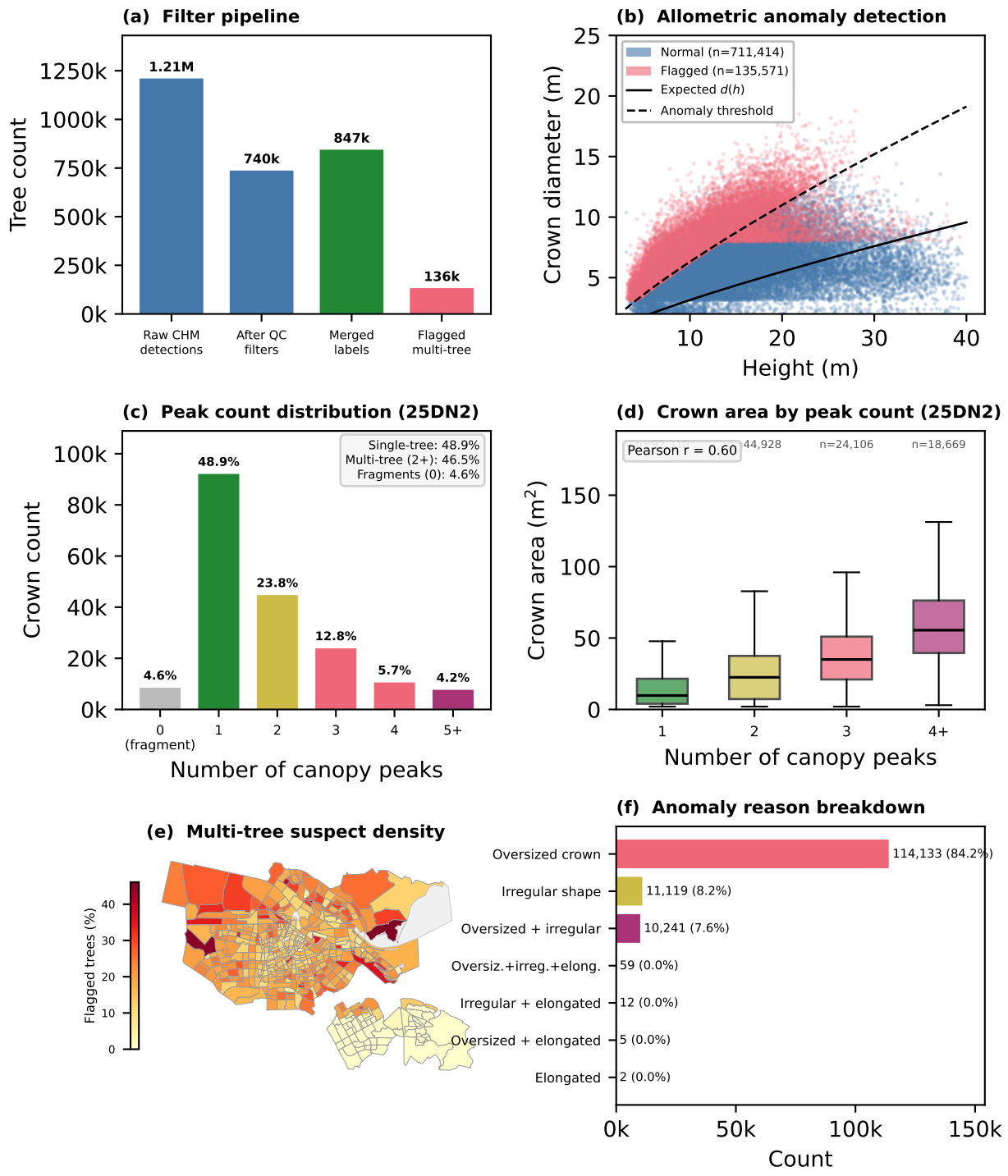

Figure S2: **Dense canopy analysis.** (a) Detection-pipeline funnel: ∼1.21 M raw CHM detections filter to 739,937 detected crowns, and the BOMEN register re-join adds 107,048 register-only entries for 846,985 merged labels, of which 135,571 are flagged as multi-tree suspects. (b) Allometric anomaly flagging: crown diameter versus height for normal (n = 711,414) and flagged (n = 135,571) crowns, with the expected allometry $d = 0.5\,h^{0.8}$ and the 2× anomaly threshold. (c) Tier-2 peak-count distribution on the illustrative tile 25DN2 (48.9% single-tree, 46.5% multi-tree, 4.6% fragments). (d) Crown area by peak count (25DN2). (e) Spatial distribution of flagged multi-tree suspects per neighbourhood. (f) Anomaly-reason breakdown for flagged polygons.

S7 Additional Supporting Figures

Figure S3 shows the distribution of effective LAI by registration status; unregistered (CHM-only) trees are slightly less dense on average than register-matched trees, consistent with the prevalence of younger self-seeded and private-garden growth. Figure S4 reports the RGB-only DeepForest detector evaluated as a transfer baseline for cities without LiDAR; its parameter sweep is given in Table S4.

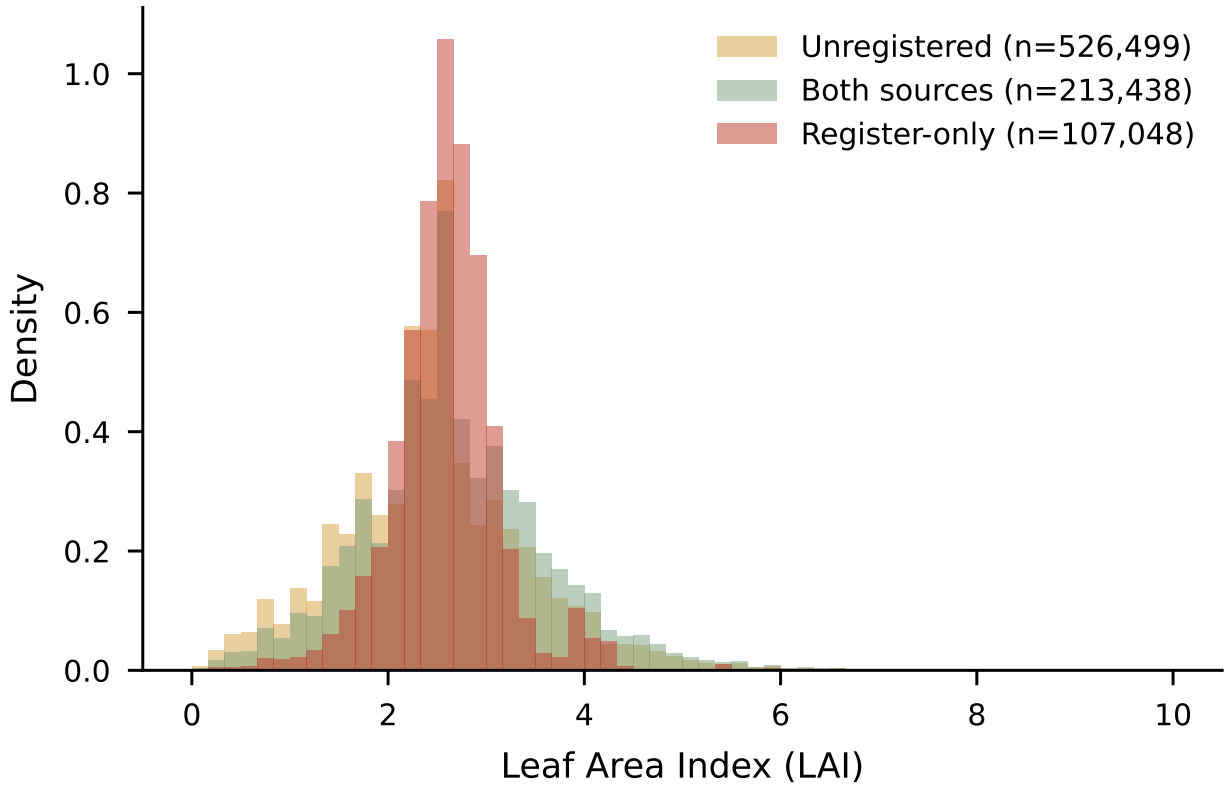

Figure S3: **LAI distribution by registration status.** LAI distribution by registration status: unregistered (mean 2.47), both-source (mean 2.67), register-only (mean 2.59). Distributions are computed from raster-derived PAI_e for every detected tree.

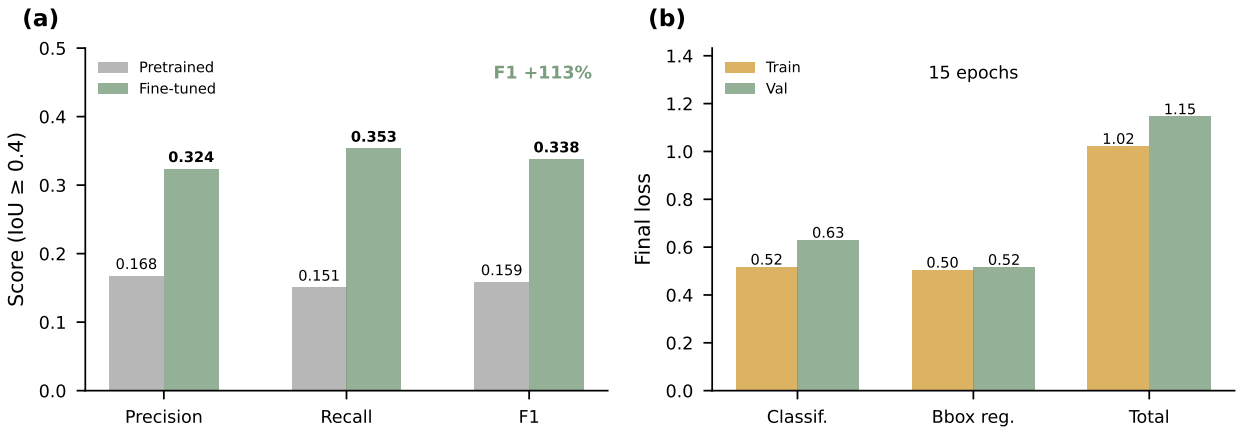

Figure S4: **DeepForest detection.** $F_1 = 0.159$ (pretrained) $\rightarrow$ 0.338 (fine-tuned), +113% relative. RGB-only fallback for cities without LiDAR; substantially below LiDAR-based watershed performance.

Table S4: DeepForest parameter tuning results. Patch size × overlap sweep on the Amsterdam dataset using spatial train/validation/test splits (70/15/15% by tile area). IoU threshold = 0.4. Best configuration highlighted.

Patch Size (px)	Overlap	Precision	Recall	F1	Notes
256	0.1	0.29	0.31	0.30	
256	0.3	0.31	0.33	0.32	
256	0.5	0.32	0.35	**0.338**	Best
384	0.1	0.28	0.30	0.29	
384	0.3	0.30	0.32	0.31	
384	0.5	0.31	0.33	0.32	
512	0.1	0.26	0.28	0.27	
512	0.3	0.28	0.30	0.29	
512	0.5	0.29	0.31	0.30	

References

[1] Hongliang Fang, Frédéric Baret, Stephen Plummer, and Gabriela Schaepman-Strub. An overview of global leaf area index (LAI): Methods, products, validation, and applications. *Reviews of Geophysics*, 57:739–799, 2019.